Hindawi Publishing Corporation
International Journal of Rotating Machinery
Volume 2012, Article ID 463585, 9 pages
doi:10.1155/2012/463585

Research Article

Effect of Inlet Geometry on Fan Performance and Flow Field in a Half-Ducted Propeller Fan

Pin Liu,[1] Norimasa Shiomi,[1] Yoichi Kinoue,[1] Ying-zi Jin,[2] and Toshiaki Setoguchi[1]

[1] *Department of Mechanical Engineering, Saga University, 1 Honjo-machi, Saga 840-8502, Japan*
[2] *Institute of Mechatronics, Zhejiang Sci-Tech University, Xiasha Higher Educational Zone, Hangzhou 310018, China*

Correspondence should be addressed to Norimasa Shiomi, siomi@me.saga-u.ac.jp

Received 6 September 2011; Revised 10 January 2012; Accepted 12 January 2012

Academic Editor: R. G. Kirk

In order to clarify the effect of rotor inlet geometry of half-ducted propeller fan on performance and velocity fields at rotor outlet, the experimental investigation was carried out using a hotwire anemometer. Three types of inlet geometry were tested. The first type is the one that the rotor blade tip is fully covered by a casing. The second is that the front one-third part of blade tip is opened and the rest is covered. The third is that the front two-thirds are opened and the rest is covered. Fan test and internal flow measurement at rotor outlet were conducted about three types of inlet geometry. At the internal flow measurement, a single slant hotwire probe was used and a periodical multisampling technique was adopted to obtain the three-dimensional velocity distributions. From the results of fan test, the pressure-rise characteristic drops at high flowrate region and the stall point shifts to high flowrate region, when the opened area of blade tip increases. From the results of velocity distributions at rotor outlet, the region with high axial velocity moves to radial inwards, the circumferential velocity near blade tip becomes high, and the flow field turns to radial outward, when the opened area increases.

1. Introduction

A lot of axial fans, which are small size and low pressure rise, are used in our daily life. Some common examples are a room ventilation fan, a radiator fan in car engine room, a cooling fan of outdoor unit of a room air conditioner, a power unit cooling fan of personal computer, and so on. They are classified into several types using the relationship of relative location between rotor blade raw and outer casing. The authors call these classified types as follows: they are ducted type, half-ducted type, semiopen type, and open type, as shown in Figure 1. The semiopen type fan, which is test fan type, has the outer casing only rear part of rotor blade tip region. In cases of semiopen type fan, inflow direction is axial and radial, that is, a part of blade tip works as blade leading edge. This inflow pattern causes complex flow at rotor inlet.

It is well known that the vortices in fans have a large effect on fan performance and its noise level. Therefore, many researches [1–7] for the vortices in fans have been conducted. However, these researches are mainly archived for the ducted type fans, while for other types of fans there are few researches.

There are studies for low-pressure axial fans as follows. For the room ventilation fan, Fukano et al. [8, 9] have clarified experimentally its aerodynamics and aeroacoustic characteristics in various relations of axial locations between rotor and outer casing. For the cooling fan of the outer unit in room air conditioner, Jang et al. [10, 11] have clarified the unsteady flow field with vortices using LDA measurement and the natures of vortices using numerical simulation. For the propeller fan without outer casing, Kato et al. [12] have numerically analyzed the relationship between vortices and noise level using LES. Also, Cai et al. [13] and Shiomi et al. [14, 15] have experimentally clarified the tip vortex behavior in opened-type axial impeller without outer casing using LDV measurement. These researches have mainly been done for relatively large rotor whose diameter is larger than 300 mm. There are a few studies on the flow fields with vortices in small cooling fan whose diameter is less than 200 mm.

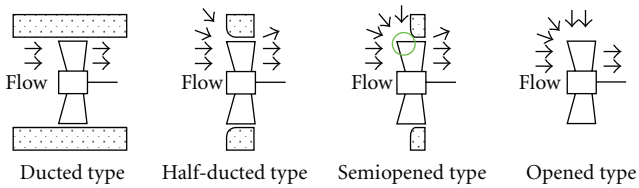

Figure 1: Types of small axial fan and image of inlet flow pattern.

In case of a ducted and a half-ducted type fan, there exists clearance between rotor blade tip and outer casing. Its clearance is called "tip clearance (TC)". Therefore, the flow occurs over the blade tip from blade pressure surface to suction surface. Its flow is called "tip leakage flow." The "tip leakage vortex" is formed by the interaction of main flow and tip leakage flow. It has been found that this vortex works as the blockage factor and causes the noise by the interaction between its vortex and some structures at downstream region. In case of open type fan, there is not the tip leakage flow because the tip clearance does not exist. In spit of its flow, the radial inflow from blade tip exists. It is found that this radial inflow becomes strong near blade suction side. Therefore, the "tip vortex" is formed by the interaction of the main flow and radial inflow near blade suction surface. In case of semiopen type fan, there is the possibility that these tow vortices exist, because in this type the front part of rotor blade tip is open type and the rear part of blade tip is covered with casing. Therefore, it is thought that the flow field near blade tip of semiopen type fan is very complex.

The final goal of this study is to develop the small axial fan with high cooling performance and low noise level. The purpose of the present study is to investigate the internal flow fields with vortices, which have large influence on machine performance and noise characteristic, and to clarify the effect of inlet geometry on the internal flow fields. Three types of the fan with different inlet geometry were tested. Those are called "TypeA," "TypeB," and "TypeC" in this paper. TypeA fan is a half-ducted type fan, and TypeB and TypeC fan are semiopened type fan. The front 1/3 region of blade tip of TypeB fan is opened and the front 2/3 region of blade tip of TypeC fan is opened. The three-dimensional velocity fields at rotor outlet were measured using a single slant hot-wire probe for each fan. The effect of inlet geometry on fan characteristics was discussed in this paper.

2. Experimental Apparatus and Procedure

Figure 2 shows the schematic view of the test rig and its component list. The section geometry of the test rig is rectilinear and its size is 880 mm × 880 mm. The flow direction is left to right shown in Figure 2. The test fan was set at no. 1 in Figure 2. It is at inlet part of test rig, so the static air of outside region flows into the test rig passing through the test fan. The flow condition at fan inlet (test rig inlet) changes with change of flowrate. The experimental condition in this paper is, therefore, shown using the flowrate.

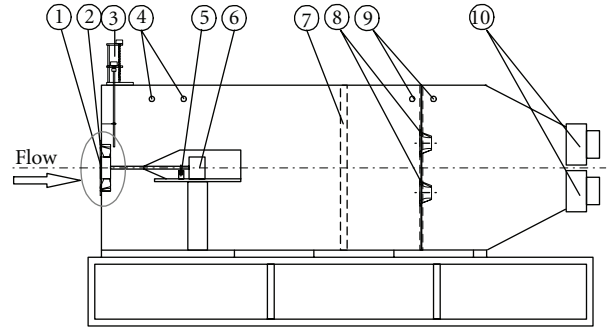

(1) Test fan
(2) Outer casing
(3) Hotwire traverse
(4) Static pressure taps
(5) Photosensor
(6) Main motor
(7) Gauge screens
(8) Nozzles
(9) Pressure taps
(10) Booster fan

Figure 2: Schematic view of test rig and its components list.

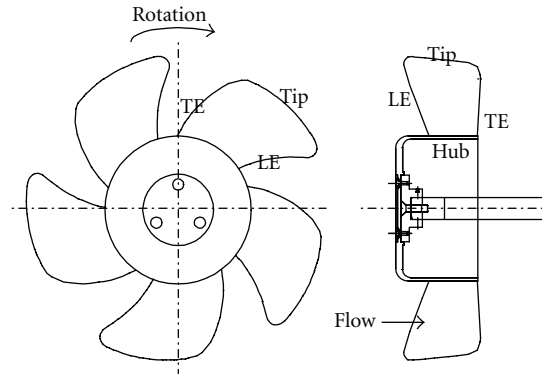

Figure 3: Outlines of test rotor.

The pressure-flowrate characteristic was clarified prior to the detailed flow measurement in order to determine the measurement flowrate. The static pressure rise was obtained from the pressure measured at the pressure taps (no. 4, in Figure 2), and the flowrate was calculated from the difference pressure between the pressure upstream and downstream of nozzle (no. 9, in Figure 2). This test rig did not have damper system, so the flowrate was varied with controlling the booster fan revolution.

Figure 3 shows the outline of the test rotor. This rotor has 5 rotor blades, its tip diameter is 180 mm, and its hub-to-tip ratio is 0.51. The tip clearance in the experiments is constant at 1.0 mm.

Figure 4 shows the schematic views of inlet geometries for test fan and the details of measurement stations. Three types of inlet geometry were tested. In this paper, they are called as TypeA, TypeB, and TypeC, respectively. TypeA fan is half-ducted type as shown in Figure 4(a). TypeB and TypeC fans are semiopened type fan. In case of TypeB, the front 1/3 part of rotor blade tip is opened as shown in Figure 4(b).

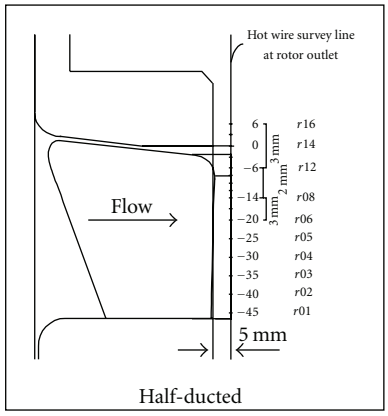

(a) TypeA

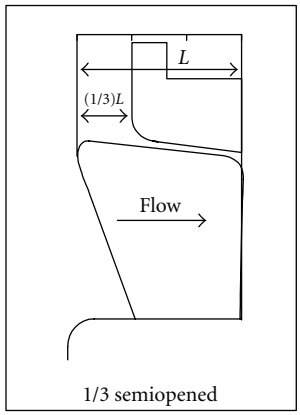

(b) TypeB

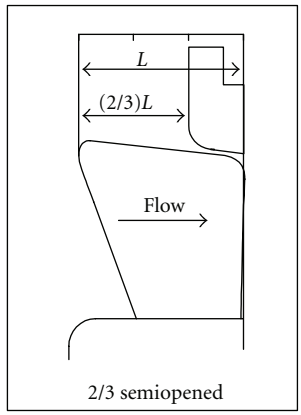

(c) TypeC

Figure 4: Inlet geometry of test fans and measurement stations of hotwire survey at rotor outlet.

In case of TypeC, the front 2/3 part of rotor blade tip is opened as shown in Figure 4(c).

The hotwire probe was traversed at 5 mm downstream of rotor. The measurement stations on each survey line are 16 stations. The velocity fields at rotor outlet were measured using a single slant hotwire probe and periodic multisampling technique developed by Kuroumaru et al. [16], for each measurement station. At each measurement station, the hotwire probe was rotated about its axis 360 degrees at interval of 14.4 degrees. The hotwire used was tungsten wire, its sensitive length was 1 mm, and its diameter was 5 μm.

The data were processed by the use of phase-locked averaging technique based on the rotor blade phase. It is the similar method used by Inoue et al. [2–4]. The rotor blade phase was obtained from the output signal of the photosensor (no. 5, in Figure 2) mounted on rotor shaft.

At the experiment, blade rotating speed was constant at 3000 rpm, and the test Reynolds number based on blade tip speed and blade chord length at midspan was 1.32×10^5.

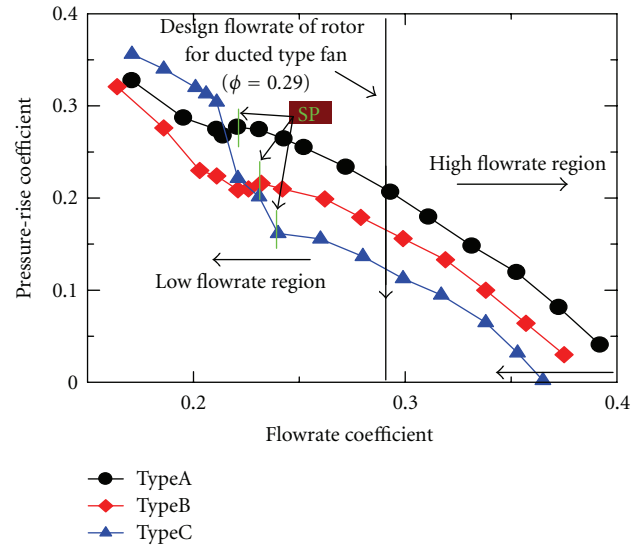

Figure 5: Pressure-flowrate characteristics for 3 types of fan.

3. Experimental Results and Discussion

Fan test and velocity measurement at rotor outlet using a hot-wire probe was done, and pressure-flowrate characteristic, the distributions of time-mean velocity component along radius, and the distributions of phase-lock averaged velocity component are shown. The effect of inlet geometry on fan characteristics and flow fields is discussed based on those results.

3.1. Pressure-Flowrate Characteristics. Figure 5 shows the pressure-flowrate characteristic curves of three types of test fan. The abscissa is flowrate coefficient, ϕ, and the ordinate is pressure-rise coefficient, ψ. The symbol in this figure is corresponded with fan type; that is, circle mark indicates the result of TypeA, diamond mark is TypeB, and triangle mark is TypeC, respectively. The definitions of flowrate and pressure coefficients are shown, respectively as follows:

$$\phi = \frac{V_a}{U_t},$$
$$\psi = \frac{P}{(1/2)\rho U_t^2}, \quad (1)$$

where V_a is the mean axial velocity passing through the rotor, U_t is the blade tip speed, P is the static pressure rise, and ρ is the air density, respectively.

The pressure coefficient becomes small as the rotor shifts forward. In general, the pressure difference between blade suction surface and pressure surface becomes large at the blade tip for ducted fan. As the test rotor is designed using a design method of ducted fan, it works mainly at blade tip region. However, in case of semiopened fan, its effectively working region becomes small because the front region of blade tip is opened. It is a reason why the pressure rise becomes small as the rotor shifts forward.

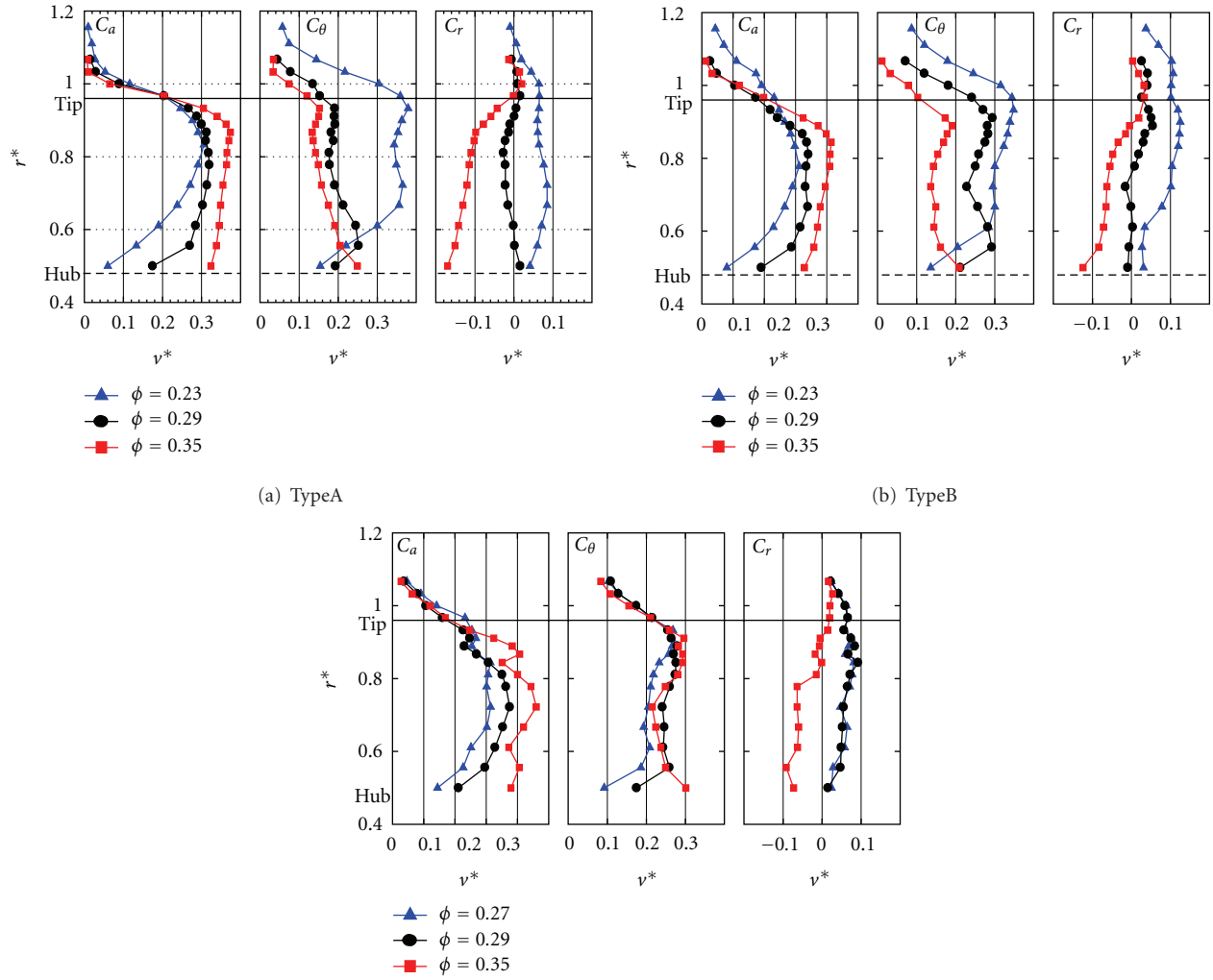

(a) TypeA

(b) TypeB

(c) TypeC

Figure 6: Distributions of time-mean velocity component along radius for three types of fan at rotor outlet.

At the high flowrate region, the maximum flowrate becomes small from over 0.400 in case of TypeA to 0.360 in case of TypeC as the rotor shifts forward. And at the low flowrate region, the stall point ("SP" in Figure 5) moves to large flowrate condition, that is, the stall margin becomes small, as the rotor shifts forward. Also, the pressure curves for TypeA and TypeB are almost the same tendency at all flowrate conditions, but the one for TypeC shows different tendency at low flowrate region.

The internal flow measurements at rotor outlet were mainly carried out at $\phi = 0.290$ for all types of fan. This is the reference flow condition in this paper. At small flowrate region, the flow fields at $\phi = 0.230$ for TypeA and TypeB fans and at $\phi = 0.270$ for TypeC fan were measured, respectively. At large flowrate region, the flow fields at $\phi = 0.350$ for all types of fan were measured.

3.2. Time-Mean Velocity Distributions along Radius. Figure 6 shows the distributions of time-mean velocity component along radius for three inlet geometries at rotor outlet. Figure 6(a) shows the results of TypeA for three flowrate conditions, Figure 6(b) shows TypeB, and Figure 6(c) shows TypeC. For each figure, the left-side figure is the distributions of nondimensional axial velocity component, C_a, the middle figure is the nondimensional circumferential velocity component, C_θ, and the right-side figure shows the nondimensional radial velocity component, C_r, respectively. Those velocity components are normalized by the blade tip speed, U_t. The x-axis indicates the nondimensional velocity, v^*, and the y-axis indicates the nondimensional radius, r^*. The marks in these figures show the flowrate conditions, respectively. "Tip" in Figure 6 indicates the location of rotor blade tip at rotor trailing edge and "Hub" in Figure 6 indicates the one of rotor hub. And $r^* = 1.0$ is the location of exit inner radius of outer casing in case of TypeA.

In case of TypeA (Figure 6(a)), the axial velocity (left-side figure of Figure 6(a)) becomes small and the location of maximum velocity moves to radial inwards when

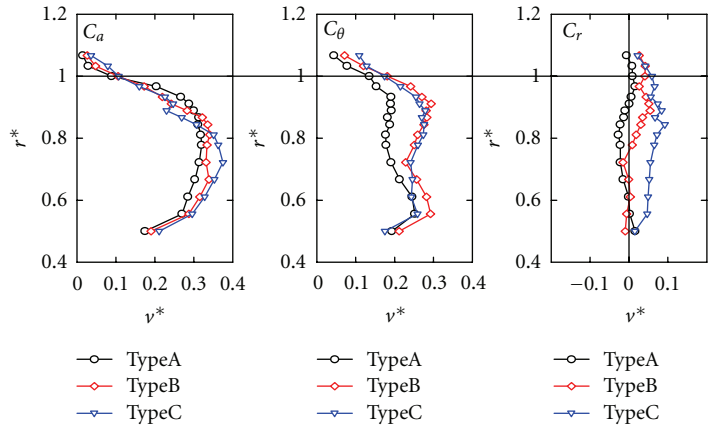

Figure 7: Comparison of the effect of inlet geometry on time-mean velocity distributions at $\phi = 0.290$.

the flowrate becomes small. And the decrease rate of axial velocity becomes large.

The velocity at outside of blade tip ($r^* > 1.0$) rapidly decreases at all flowrate conditions, and its value becomes almost the zero. The circumferential velocity (middle figure of Figure 6(a)) becomes large when the flowrate is small. In this case, the circumferential velocity at $\phi = 0.230$ becomes dramatically large, but its value becomes small near hub. The radial velocity (right-side figure of Figure 6(a)) becomes large when the flowrate is small. At $\phi = 0.350$, the radial velocity inside the blade tip region ($r^* < 1.0$) is all minus value. It means that the air flow turns to radial inwards and the flow fields become contraction. At $\phi = 0.290$, the radial velocity inside the blade tip region ($r^* < 1.0$) is almost the zero. It means that the air flow at rotor outlet is almost the parallel to rotor axis. And, at $\phi = 0.230$, the radial velocity on all radial location at rotor outlet is pulse value, that is, the air flow turns to radial outwards, but its value is almost zero near hub. As the axial, circumferential and radial velocity near hub become very small at $\phi = 0.230$, it is considered that the dead flow region is formed near hub in this flowrate condition. It is similar to hub-corner stall in axial compressor reported by Lei et al. [17].

In case of TypeB (Figure 6(b)), the tendency of axial velocity profiles (left-side figure in Figure 6(b)) is almost the same one in case of TypeA. A little difference, however, exists near blade tip region at $\phi = 0.230$. The circumferential velocity (middle figure in Figure 6(b)) gradually increases as the flowrate is smaller. The circumferential velocity near blade tip ($0.8 < r^* < 1.0$) becomes large. Inoue et al. [3], have reported that the similar velocity distribution was observed in axial compressor rotor and have shown that it is due to the tip leakage vortex. The tendency of radial velocity (right-side figure in Figure 6(b)) in case of TypeB is almost the same one in case of TypeA. The minus value of radial velocity inside the blade tip at $\phi = 0.350$ is a little smaller than the one of TypeA. It means that the rate of contraction becomes small compared with the results of TypeA. At $\phi = 0.290$, the value of radial velocity at the region of $r^* > 0.8$ becomes pulse. At $\phi = 0.230$, the value of radial velocity becomes pulse at all radial measurement stations.

In case of TypeC (Figure 6(c)), the axial velocity distributions for all flowrate conditions (left-side figure in Figure 6(c)) have local decline near blade tip region. The circumferential velocity distributions (middle figure in Figure 6(c)) have large value at $r^* < 1.0$ at all flowrate condition. The radial velocity distribution (right-side figure in Figure 6(c)) at $\phi = 0.290$ shows positive value at all radial location. It means that the flow field turns to radial outward and it is similar to near stall condition of TypeA and TypeB.

Figure 7 shows the comparison of effect of inlet geometry on the distributions of time-mean velocity component along radius at rotor outlet at $\phi = 0.290$. The left-side figure of Figure 7 shows distribution of nondimensional axial velocity component, the middle figure of Figure 7 shows nondimensional circumferential velocity, and the right-side figure of Figure 7 shows nondimensional radial velocity, respectively. The abscissa of each figure is nondimensional velocity, v^*, and the ordinate is nondimensional radius, r^*. The marks in figure indicate the inlet geometry, respectively.

For the axial velocity, in case of TypeA the radial location that obtained maximum velocity is near $r^* = 0.85$. Its location shifts to radial inward from TypeA to TypeC. Those locations are near $r^* = 0.8$ for TypeB and it is near $r^* = 0.7$ for TypeC. As the open region of blade tip enlarges, the mass of radial inflow increases. Therefore, the main flow region moves to radial inward. Also, the value of maximum velocity becomes large from TypeA to TypeC. It means that the area of main flow region becomes small according to continuity equation. The circumferential velocity of TypeB and TypeC becomes larger near blade tip than the one of TypeA. The circumferential velocity becomes large at the region that the axial velocity rapidly decreases, especially its tendency is remarkable for TypeB and TypeC. As it is known that the circumferential velocity becomes large at the region with vortex reported by Inoue et al. [3], it is possible that the strong vortex exists near blade tip for TypeB and TypeC. For the radial velocity, the distribution of TypeB is similar to TypeA near hub and similar to TypeC near blade tip.

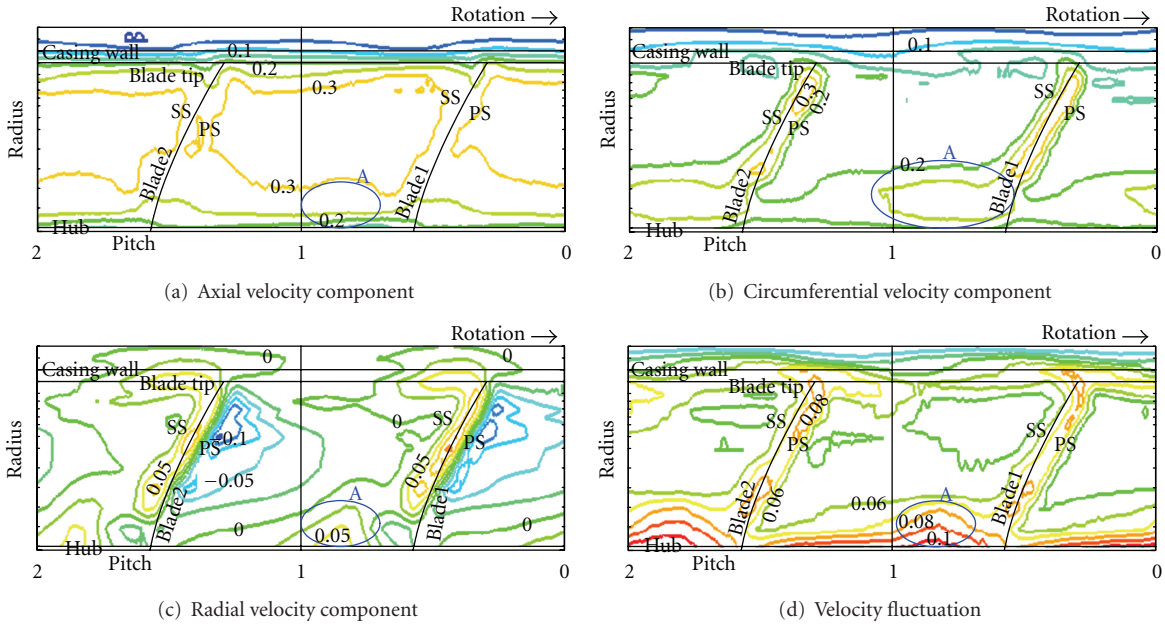

(a) Axial velocity component

(b) Circumferential velocity component

(c) Radial velocity component

(d) Velocity fluctuation

Figure 8: Contour maps of each velocity component and velocity fluctuation at rotor outlet of TypeA at $\phi = 0.290$.

3.3. Phase-Lock Averaged Velocity Distributions. Figures 8(a)–8(d) show the contour maps of axial, circumferential, radial velocity component, and velocity fluctuation at rotor outlet for TypeA at $\phi = 0.290$. The abscissa is pitch-wise direction and the ordinate is radial direction, respectively. The value of velocity in each figure is normalized by the blade tip speed, U_t. Blade rotating direction is from left to right as shown at top-right side of the figure. "SS" in each figure means blade "suction surface" and "PS" means blade "pressure surface", respectively.

As a result, the flow field for TypeA at $\phi = 0.290$ is the appropriate flow field because it is similar to the one which can be expected. The axial velocity (Figure 8(a)) inside the blade passage is almost uniform. Compared with its distribution near blade SS and PS, the span-wise extent of uniform velocity area for blade SS is a little larger than the one for blade PS. For circumferential velocity distribution (Figure 8(b)), the velocity inside the blade passage is almost uniform. It is found that the circumferential velocity becomes clearly large at blade wake region. For radial velocity distribution (Figure 8(c)), the flow field on blade PS turns to radial inwards and the one on blade SS turns to radial outward. As the value of radial velocity is almost the zero inside the blade passage. For velocity fluctuation (Figure 8(d)), there does not exist the area with large fluctuation inside the blade passage. The velocity fluctuation becomes high at blade wake region. Observing the flow field at detail, the circumferential velocity becomes a little large at the region of hub-blade SS corner (marked area, "A"). In this region, the axial velocity contour line is slightly distorted, the value of radial velocity component becomes large, and the velocity fluctuation becomes high. This shows the influence of hub-corner separation on flow field discussed by Lei et al. [17]. And, from these results, the effect of vortex on the flow field is hardly observed at rotor outlet of TypeA fan at $\phi = 0.290$.

Figures 9(a)–9(d) show the contour maps of three directional velocity components and velocity fluctuation at rotor outlet for TypeB at $\phi = 0.290$. The abscissa, the ordinate, and so on are the same ones in Figure 8.

Compared with the results of TypeA, the uniformity of flow field is distorted. The axial velocity (Figure 9(a)) becomes small near both of the hub-blade corners inside the blade passage. The velocity decreasing near hub-blade SS corner is thought due to the effect of the hub-corner separation. Therefore, the area of hub-corner separation for TypeB becomes larger than the one for TypeA. It is confirmed from the result of circumferential velocity (Figure 9(b)) that the region with large circumferential velocity at the corner of rotor hub and blade SS (marked area, "B") enlarges compared with the one of TypeA. In this region, radial velocity becomes large and velocity fluctuation becomes high. Another large difference from the result of TypeA is observed in the region on blade PS near blade tip (marked area, "C"). In this region, circumferential velocity becomes large. It means that the flow in this region entrained with the blade rotation. Velocity fluctuation in this region is also high. Tip vortex and/or tip leakage vortex, therefore, exists on a blade SS near blade tip as shown by Jang et al. [10, 11]. Its vortex moves to downstream with the flow diagonally across the blade passage. However, the vortex interacts with the blade PS of next blade before it reaches to the location of blade trailing edge. The vortex is broken and its disturbance propagates along the blade PS to downstream region. It is the similar phenomenon as vortex breakdown occurred in axial compressor rotor clarified by Furukawa et al. [6]. The fluctuations flow out from the blade with almost the same circumferential velocity as rotor blade rotating.

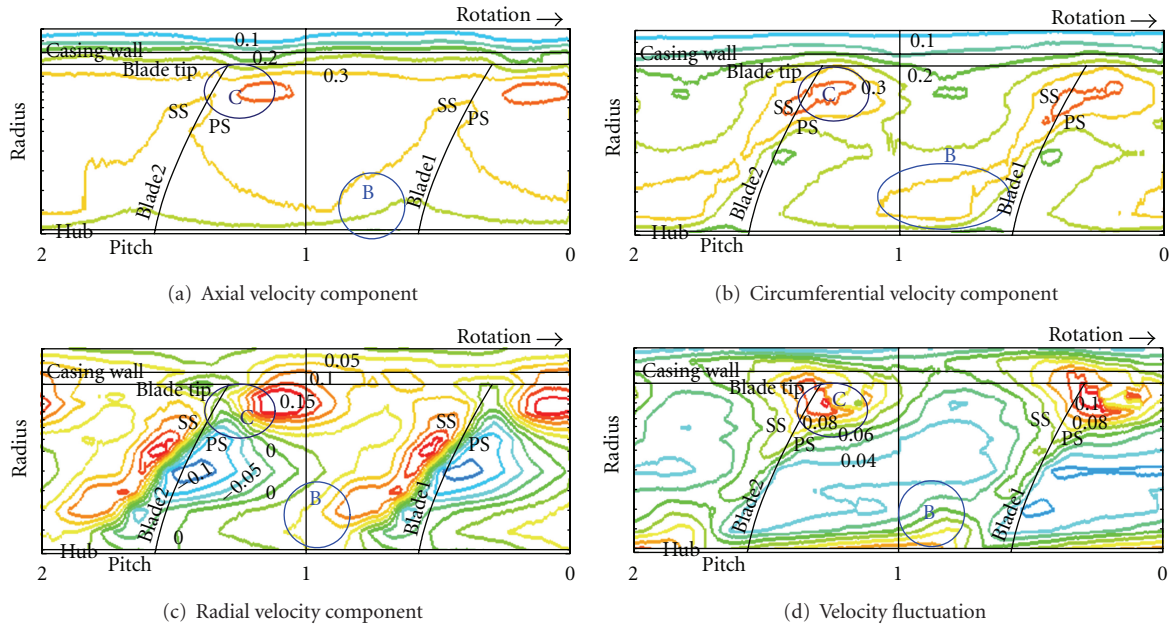

(a) Axial velocity component

(b) Circumferential velocity component

(c) Radial velocity component

(d) Velocity fluctuation

Figure 9: Contour maps of each velocity component and velocity fluctuation at rotor outlet of TypeB at $\phi = 0.290$.

Therefore, the large circumferential velocity and the high velocity fluctuation are observed in this region. One more interest flow pattern exists in radial velocity distribution (Figure 9(c)). Radial velocity becomes very large at the right-top side of area "C". When the counter clock-wise vortex exists, generally, radial velocity turns to radial outwards at the right-side area of its vortex and turns to radial inwards at the left-side area of it. If it is so, this region with large radial velocity is the one including the effect of vortex. That is, in the case of TypeA at $\phi = 0.290$, the vortex is not broken completely, and its effect remains still strongly.

Figures 10(a)–10(d) show the contour maps of three directional velocity components and velocity fluctuation at rotor outlet for TypeC at $\phi = 0.290$. The abscissa, the ordinate, and so on are the same ones in Figures 8 and 9.

At first, it must be noted that the flow condition for TypeC at $\phi = 0.290$ is different from the one for TypeA and TypeB, although the measurement flowrate is the same. From the result of pressure-flowrate characteristic, the flow field of TypeC at $\phi = 0.290$ is similar to the one near stall point. For axial velocity (Figure 10(a)), the main flow region is limited around blade midspan. The axial velocity becomes small near blade tip. From the result of circumferential velocity (Figure 10(b)), the region with large circumferential velocity enlarges near blade tip region from blade PS to blade midpitch. And, in this region, velocity fluctuation becomes high (Figure 10(d)). Therefore, there exists something that brocks the axial flow.

3.4. Discussion on Effect of Inlet Geometry. From the result of fan test, the fan performance becomes wrong with change of inlet geometry from TypeA to TypeC. This tendency is similar to the case with increasing tip clearance at ducted type fan, reported by Cai et al. [18]. At the ducted fan, the mass of leakage flow increases as tip clearance becomes large. The leakage flow does not have a radial velocity component, but has a strong circumferential velocity component. In the test fan, as the opened area outside of blade tip become large from TypeA to TypeC, the flow with a strong radial velocity component flows into the blade passage passing through blade tip. Although the vortex is formed for both ducted and semiopened fan (in this paper, they are TypeB and TypeC), its vortex is tip leakage vortex for ducted fan and tip vortex for semiopened fan. The basic mechanism to make vortex is almost the same, that is, the flow interaction between the main flow and the radial inflow passing through blade tip.

From the results of internal flow measurement, the flow fields of TypeA at $\phi = 0.290$ is near ideal condition because the disturbance by vortex or corner stall is hardly observed. On the other hand, the flow fields of TypeB and TypeC have several disturbances near blade tip and hub-blade SS corner. The disturbance near blade tip of TypeC is very large. Furukawa et al. [6] reported the phenomena of the vortex breakdown in an axial compressor. In this, the vortex breakdown occurs when the blade loading increases. It is, therefore, considered that the blade loading near blade tip of TypeC becomes high compared with the one of TypeB. It is because the opened area outside of blade tip expands and because the mass of radial inflow increases. Therefore, the interaction of the main flow and the radial inflow is strengthened.

4. Conclusions

In a half-ducted small axial fan, the fan test and the internal flow measurement at rotor outlet were carried out for three kinds of different inlet geometry, one is half-ducted type

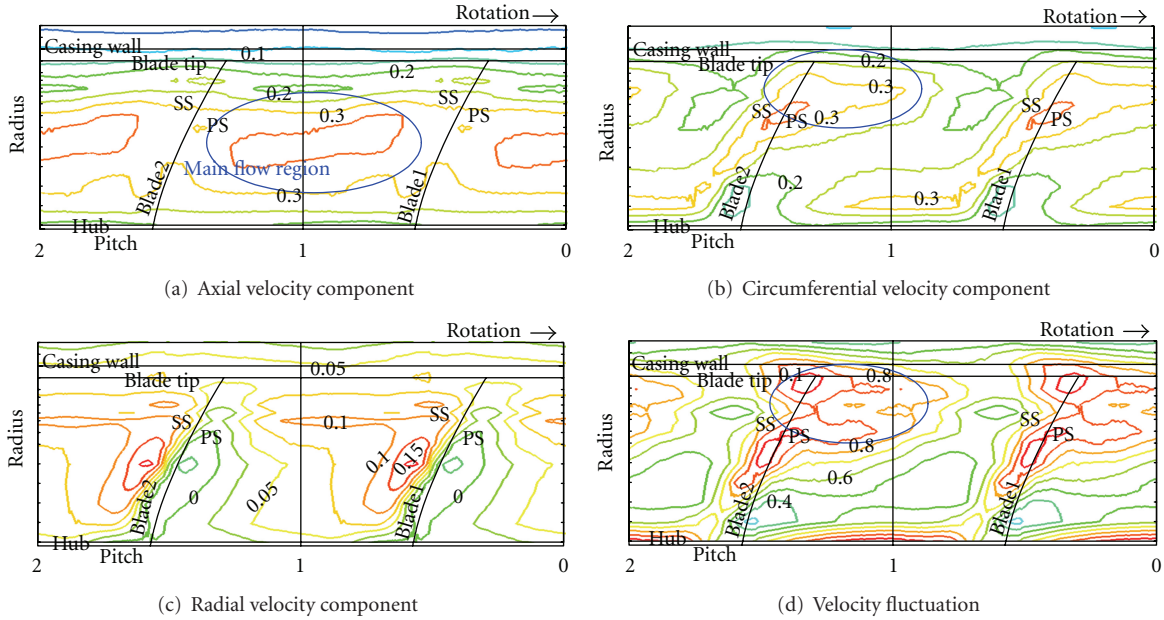

(a) Axial velocity component

(b) Circumferential velocity component

(c) Radial velocity component

(d) Velocity fluctuation

Figure 10: Contour maps of each velocity component and velocity fluctuation at rotor outlet of TypeC at $\phi = 0.290$.

and the others are semiopened types. The effect of these inlet geometries on fan characteristic and three-dimensional velocity fields at rotor outlet were discussed. The main conclusions are as follows.

(1) From the results of fan test, the pressure rise becomes small and the stall point shifts to large flowrate condition with change of inlet geometry from TypeA to TypeC.

(2) The location of maximum value of time-mean axial velocity at $\phi = 0.290$, which is design flowrate of rotor, moves to radial inwards with change of inlet geometry from TypeA to TypeC.

(3) Time-mean circumferential velocity near blade tip for TypeB and TypeC at $\phi = 0.290$ is larger than the one of TypeA. This is because the effect of vortex strongly appeared.

(4) The flow field turns to radial outwards at $\phi = 0.290$ with change of inlet geometry from TypeA to TypeC.

(5) At small flowrate condition, the effect of hub-corner stall is observed for all inlet geometries.

(6) For TypeA fan, the flow field at $\phi = 0.290$ shows the good condition because the influence of vortex is hardly observed.

(7) For TypeB fan, the strong effect of vortex is observed near blade tip region at $\phi = 0.290$.

(8) For TypeC fan, its flow field is similar to the one near stall point even at $\phi = 0.290$.

Nomenclature

C_a: Nondimensional axial velocity ($=V_a/U_t$)
C_θ: Nondimensional circumferential velocity ($=V_\theta/U_t$)
C_r: Nondimensional radial velocity ($=V_r/U_t$)
LE: Leading edge of rotor blade
PS: Pressure surface of rotor blade
r: Radius [m]
r_{tip}: Tip radius of rotor blade (=0.09 [m])
r^*: Nondimensional radius ($=r/r_{tip}$)
SS: Suction surface of rotor blade
TC: Tip clearance
TE: Trailing edge of rotor blade
TLV: Tip leakage vortex
U_t: Rotor tip speed (=28.6 [m])
V_a: Axial velocity [m/s]
V_θ: Circumferential velocity [m/s]
V_r: Radial velocity [m/s]
ϕ: Flowrate coefficient
θ: Circumferential direction
ρ: Density of air
ψ: Pressure-rise coefficient.

References

[1] S. Leibovich, "The structure of vortex breakdown," *Annual Review of Fluid Mechanics*, vol. 10, pp. 211–246, 1978.

[2] M. Inoue and M. Kuroumaru, "Three dimensional structure and decay of vortices behind an axial flow rotating blade row," *Journal of Engineering for Gas Turbines and Power*, vol. 106, no. 3, pp. 561–569, 1984.

[3] M. Inoue, M. Kuroumaru, and M. Fukuhara, "Behaviour of tip leakage flow behind an axial compressor rotor," *Journal of*

Engineering for Gas Turbines and Power, vol. 108, no. 1, pp. 7–14, 1986.

[4] M. Inoue and M. Kuroumaru, "Structure of tip clearance flow in an isolated axial compressor rotor," *Journal of Turbomachinery*, vol. 111, no. 3, pp. 250–256, 1989.

[5] B. Lakshminarayana, M. Zaccaria, and B. Marathe, "The structure of tip clearance flow in axial flow compressors," *Journal of Turbomachinery*, vol. 117, no. 3, pp. 336–347, 1995.

[6] M. Furukawa, M. Inoue, K. Saiki, and K. Yamada, "The role of tip leakage vortex breakdown in compressor rotor aerodynamics," *Journal of Turbomachinery*, vol. 121, no. 3, pp. 469–480, 1999.

[7] R. Mailach, I. Lehmann, and K. Vogeler, "Rotating instabilities in an axial compressor originating from the fluctuating blade tip vortex," *Journal of Turbomachinery*, vol. 123, no. 3, pp. 453–463, 2001.

[8] T. Fukano, M. Fukuhara, K. Kawagoe, Y. Hara, and K. Kinoshita, "Experimental study on the noise reduction of a propeller fan (1st Report, Aerodynamic Characteristics)," *Transactions of the Japan Society of Mechanical Engineers*, vol. 56–531, pp. 3378–3382, 1990 (Japanese).

[9] T. Fukano, K. Kawagoe, M. Fukuhara, Y. Hara, and K. Kinoshita, "Experimental study on the noise reduction of a propeller fan (1st Report, Aerodynamic Characteristics)," *Transactions of the Japan Society of Mechanical Engineers*, vol. 56–531, pp. 3383–3388, 1990 (Japanese).

[10] C. M. Jang, M. Furukawa, and M. Inoue, "Analysis of vortical flow field in a propeller fan by LDV measurements and LES—part I: three-dimensional vortical flow structures," *Journal of Fluids Engineering*, vol. 123, no. 4, pp. 748–754, 2001.

[11] C. M. Jang, M. Furukawa, and M. Inoue, "Analysis of vortical flow field in a propeller fan by LDV measurements and LES—part II: unsteady nature of vortical flow structures due to tip vortex breakdown," *Journal of Fluids Engineering*, vol. 123, no. 4, pp. 755–761, 2001.

[12] C. Kato, S. Shishido, M. Miyazawa, H. Yoshiki, H. Ito, and H. Tsubota, "Numerical prediction of aerodynamic noise radiation from a propeller fan," in *Proceedings of the 5th KSME-JSME Thermal and Fluids Engineering Conference*, pp. 522–527, 2002.

[13] W. X. Cai, N. Shiomi, K. Sasaki, K. Kaneko, and T. Setoguchi, "Visualization of tip vortex flow in an open axial fan by EFD," *Journal of Visualization*, vol. 5, no. 3, pp. 293–300, 2002.

[14] N. Shiomi, K. Kaneko, W.-X. Cai, K. Sasaki, and T. Setoguchi, "Tip vortex feature in an open axial fan," *Turbomachinery*, vol. 31, no. 9, pp. 545–553, 2003.

[15] N. Shiomi, K. Kaneko, and T. Setoguchi, "Effect of inlet geometry on the flow fields around rotor in a small axial fan," in *Proceedings of the International Symposium on Transport Phenomena and Dynamics of Rotating Machinery (ISROMAC '06)*, Hawaii, Hawaii, USA, 2006.

[16] M. Kuroumaru, M. Inoue, T. Higaki, A.-E. Farouk, and T. Ikui, "Measurement of three-dimensional flow field behind an impeller by means of periodic multi-sampling of a slanted hot wire," *Transactions of the Japan Society of Mechanical Engineers B*, vol. 48, no. 427, pp. 408–417, 1982 (Japanese).

[17] V. M. Lei, Z. S. Spakovszky, and E. M. Greitzer, "A criterion for axial compressor hub-corner stall," *Journal of Turbomachinery*, vol. 130, no. 3, Article ID 031006, 10 pages, 2008.

[18] W.-X. Cai, K. Kaneko, N. Shiomi, and T. Setoguchi, "The flow near rotor blade tip of high specific-speed diagonal flow fan," *Turbomachinery*, vol. 9-10, pp. 619–625, 2001 (Japanese).